

Transition from Single-to Multi-Cell Natural Convection of Air in Cavities with an Aspect Ratio of 20: A Thermodynamic Approach

Michel Pons
CNRS-LIMSI, BP 133, 91403 Orsay Cedex, France
E-mail: michel.pons@limsi.fr

Abstract

Transition from mono-cellular to multi-cellular flow in differentially heated cavities with an aspect ratio of 20 is revisited. Our numerical model is based on the Boussinesq equations, modified for including the work of pressure forces. In high enough cavities, this work has significant effects and results are changed. The Nusselt number is increased while convection is reduced, moreover all transitions are delayed. A thermodynamic analysis of transition is developed. The analysis shows that, after transition, the multi-cellular flow topology tends to decrease altogether viscous friction and work of buoyancy forces. In other words, transition weakens its own cause. This is why a threshold exists.

Keywords: natural convection, numerical model, thermodynamics, irreversibilities.

1. Introduction

Since the seminal work of Batchelor (Batchelor, 1954), thermal convection in 2-D tall differentially heated cavities (with aspect ratios $A=H/L$ above 15) has received great interest, probably because of its relevance in building engineering. Batchelor (1954) demonstrated that, sufficiently far away from the horizontal walls and when the Rayleigh number Ra is weak, the flow is 1-D, temperature T is a linear function of the horizontal position x (non-dimensional: $0 \leq x \leq 1/A$) while vertical velocity is a cubic function:

$$V_z = \frac{\alpha}{6L} Ra_L Ax(Ax - 0.5)(Ax - 1) \quad (1)$$

This is the *conduction* regime. It is well known that beyond a critical value of the Rayleigh number [$Ra_L = \beta g L^3 \Delta T (\alpha \nu)^{-1}$] the flow undergoes transition from single- to multi-cell pattern. Inside the external primary cell, secondary cells appear along the midline of the cavity ($x=0.5/A$). This *transition* regime exists as stable steady-states. That transition has been studied since the 60s and still is. Experimentally, Elder (1965) investigated laminar flows in viscous fluids with aspect ratios up to 60; ElSherbiny et al. (1982) investigated laminar and turbulent air flows in inclined cavities with aspect ratios up to 110; Lartigue et al. (2000) investigated laminar air flows with the aspect ratio of 40; Betts and Bokhari (2000) investigated

turbulent air flows with the aspect ratio of 29; Wright et al. (2006) investigated laminar and turbulent air flows with the aspect ratio of 40. Numerically, De Vahl Davis and Mallinson (1975) simulated the configurations of Elder (1965) and obtained good agreement; Roux et al. (1980) investigated the return from multi-cellular to mono-cellular flow; Lee and Korpela (1983) simulated multi-cellular laminar flows in air, water or oil, with aspect ratios ranging from 15 to 40; Le Quéré (1990) simulated multi-cellular laminar air flows with aspect ratios ranging from 16 to 24 and found periodical behaviors; Zhao et al. (1997) simulated air flows with aspect ratios ranging from 11 to 50. As linear stability analyses, Birikh (1966) calculated the small perturbations of the base flow Equation (1); the perturbation consists of a series of successive and similar co-rotating cells often called "the cats eyes". Vest and Arpacı (1969) studied the conduction and boundary-layer regimes and calculated the respective secondary flows; Korpela et al. (1973) investigated the effect of the Prandtl number; Bergholz (1978) included the effect of thermal stratification; Desrayaud and Lauriat (1988) included the effect of radiation; and Chait and Korpela (1989) investigated the stability of the secondary flow.

The present study develops a thermodynamic approach of that transition. How are the thermodynamic quantities, especially the

irreversibilities, modified by transition, and what do those changes give as insight? This approach is developed on a rather simple case where the fluid is air at ambient temperature (300K, $Pr=0.71$) in a cavity of aspect ratio $A=20$. Moreover, we investigate the effect of the cavity size.

The numerical model: *thermodynamic* Boussinesq equations

The numerical model is based on the Boussinesq equations (1903), but slightly modified according to Spiegel and Veronis (1960). These authors confirm that the continuity and momentum equations of Boussinesq are thermodynamically correct, but not the heat equation. Following thermodynamic arguments, Spiegel and Veronis keep in the heat equation two terms neglected by Boussinesq: the work of pressure forces and the heat generated by viscous friction. The temperature equation, as derived from the enthalpy formulation of the heat equation, writes then:

$$\frac{DT}{Dt} = \alpha \nabla^2 T + \frac{T}{c_p} \left(\frac{\partial(\rho^{-1})}{\partial T} \right)_P \frac{DP}{Dt} + \frac{q_v}{\rho c_p} \quad (2)$$

They called the so-modified Boussinesq system, the *thermodynamic* Boussinesq equations. Indeed, these equations yield completely consistent thermodynamic balances especially with respect to the second law, when the *usual* Boussinesq equations do not (Costa, 2005; Pons and Le Quéré, 2005a, 2005b, 2007). If the two last terms of Equation (2) were neglected by Boussinesq, the *Low-Mach-Number* approximation only neglects the very last term and approximates DP/Dt by the time derivative of average pressure. We herein focus on steady-states (pressure is obviously constant) in large enough enclosures for the pressure gradient to be considered. As a first order approximation, we consider the hydrostatic gradient: $DP/Dt = -\rho_0 g V_z$. Indeed, deviations due to stratified density gradient or to hydrodynamic pressure field are of the second order.

For non-dimensionalization, our reference quantities are: the cavity height H for distances, $\alpha \sqrt{ARa_L}/L$ for velocities, their ratio for time, ΔT for the difference $T-T_0$, where $T_0=(T_h+T_c)/2$. The non-dimensional temperature equation then writes:

$$\frac{\partial \theta}{\partial \tau} + u \frac{\partial \theta}{\partial x} + w \frac{\partial \theta}{\partial z} = \frac{1}{A \sqrt{ARa_L}} \nabla^2 \theta - \phi w + \frac{\beta g H}{c_p} \left(\frac{\Phi}{A \sqrt{ARa_L}} - \theta w \right) \quad (3)$$

where $\phi = \beta g H T_0 / (c_p \Delta T)$ is the adiabatic temperature gradient $\beta g T_0 / c_p$ non-dimensionalized by the vertical temperature gradient in the problem $\Delta T / H$. The number $\beta g H / c_p$ appearing in the rightmost term is usually very small (of the order of 10^{-5} in this study). On the other hand, the term $(-\phi w)$, which is practically the work of the pressure stress, can easily be of the order of unity and therefore is better not to be neglected. The equations are solved with a finite-difference second-order scheme in time and space on a regular staggered 128×512 grid. This grid is much finer than ever done before: Lee and Korpela (1983) used a 33×33 grid, and Le Quéré (1990) a 24×120 grid. Moreover, regular grids improve resolution in the center of the cavity, there where the secondary cells form. Leonard and Drummond (1995) point out that this problem requires special care on the numerical scheme. More details about the numerical procedure are given by Pons and Le Quéré (2007). The boundary conditions are: no slip at the four walls, prescribed temperatures on the vertical walls (hot on the left side, cold on the right one), and adiabatic horizontal walls.

As the *thermodynamic Boussinesq* equations involve the parameters ϕ ($\phi \propto H / \Delta T$) and $\beta g H / c_p$, a given configuration cannot be described by the Rayleigh number only ($Ra_L \propto L^3 \Delta T$). Therefore two cavities with two given heights are considered herein: a *small* one, where the work of pressure forces will be negligible ($\phi \ll 1$) so that the *thermodynamic* and *usual* models yield similar results, and a *large* one where the work of pressure forces is not negligible (ϕ of the order of 1). The two cavities are described in TABLE 1, both are of human size, not of geophysics dimensions. It is often stated that the Boussinesq model is valid as soon as ΔT is small enough except for geophysical configurations. However, Gray and Giorgini (1976) and Velarde and Perez-Cordon (1976) demonstrated that this condition is not sufficient and that the magnitude of ϕ with respect to one must also be considered. TABLE 1 gives the values of ϕ and ΔT (corresponding to $Ra_L=5000$) investigated herein. The values of Ra_L above 5000 explored below are obtained just by keeping H constant while increasing ΔT , so that ϕ is decreased proportionally.

We started our investigation with a monocellular flow ($Ra_L=5400$ for the small cavity, $Ra_L=6200$ for the large one) and increased the

Rayleigh number by steps of 100. The non-dimensional steady-state calculated for one Rayleigh was used as initial state for the next calculation. We explored the range up to $Ra_L=8000$. Then the same procedure was followed, but descending from $Ra_L=8000$ down to the initial value. We did not find the slightest hysteresis in the results neither in terms of cell numbers nor for any thermodynamic quantity.

TABLE I. THE TWO CONFIGURATIONS INVESTIGATED HEREIN.

Cavity	H [m]	ϕ for $Ra_L=5000$	ΔT [K] for $Ra_L=5000$
<i>small</i>	0.808	0.01	0.789
<i>large</i>	2.032	0.4	0.0496

Transition

The first studies on that transition used linear stability analyses with a base flow defined by Equation (1). The critical Rayleigh Ra_L lies between 5600 and 5700 (Bergholz, 1978; Birikh, 1966; Birikh et al., 1968, 1969; Chait and Korpela, 1989; Vest and Arpaci, 1969). Purely numerical studies yielded the value 5800 (Zhao et al., 1997). As all those evaluations are based on the *usual* Boussinesq equations, they can only apply to the present *small* cavity.

Our numerical results are presented in *Figure 1*. Two secondary cells appear in the center of the small cavity at $Ra_L=5875$, which is in good agreement, although slightly above, with the linear stability analyses and previous numerical studies mentioned above. However, it must also be noticed that, as shown in *Figure 1* and already mentioned in literature, the number of secondary cells increases very rapidly from two to six (obtained at $Ra_L=6100$). The six cells survive up to $Ra_L=7100$ where a seventh cell sets on. Between $Ra_L=7200$ and $Ra_L=9000$, there are seven secondary cells in the small cavity.

The same transitions occur in the large cavity, except that the Rayleigh numbers are significantly shifted, see TABLE 2. It can be noticed that, in either cavity, the transition from one to six secondary cells takes place over a narrow Rayleigh-range ($\Delta Ra_L=200$, or 400) when the configuration with six cells survives over a much wider range ($\Delta Ra_L=1000$).

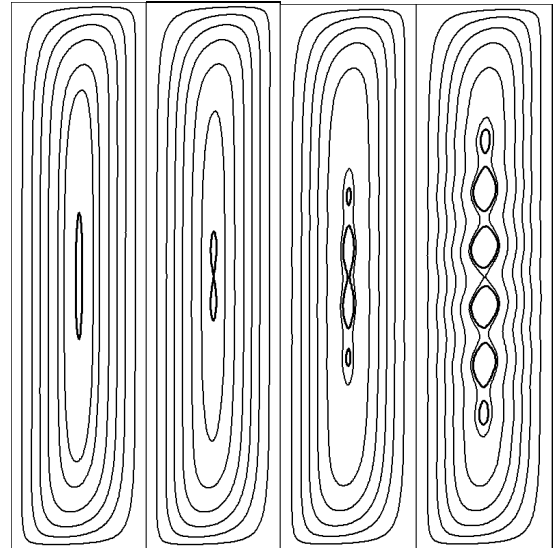


Figure 1. Flow in the small cavity for, successively, $Ra_L=5800$ (1 cell), 6000 (2 cells), 6050 (4 cells), 6200 (6 cells). The hot wall is on the left side.

TABLE II. EXISTENCE RANGE OF RAYLEIGH NUMBER FOR EACH TOPOLOGY

Cavity :	<i>small</i>	<i>large</i>
Two cells	5875-6000	6500-6600
Four cells	6050	6700-6800
Six cells	6100-7100	6900-7900
Seven cells	7200-9000	8000-9200

Moreover, although all the configurations occurring before had only an even numbers of cells, the next transition occurs from an even to an odd number of cells, the latter configuration being also very robust.

Heat fluxes, irreversibilities and transition

The thermodynamic analysis applied to this transition starts with two quantities. The first one is the Nusselt number, *i.e.* the ratio of the effective heat flux to that transferred in a purely conductive system (fluid at rest):

$$Nu = A^{-1} \int_0^1 (-\partial\theta/\partial x) dz \quad (4)$$

This quantity represents not only the global heat transfer but also the total irreversibility. Indeed, in similarity with the Nusselt number, irreversibilities can be non-dimensionalized by the total entropy production of the purely conductive system, yielding *numbers of irreversibility*. The so-defined numbers of viscous and conductive irreversibility are respectively:

$$N_{Iv} = \frac{\phi}{A} \int_{cavity} \frac{\Phi}{(1 + \theta \Delta T / T_0)} dx dz \quad (5)$$

with $\Phi = 2 \left(\frac{\partial u}{\partial x} \right)^2 + \left(\frac{\partial u}{\partial z} + \frac{\partial w}{\partial x} \right)^2 + 2 \left(\frac{\partial w}{\partial z} \right)^2$, and

$$N_{Iq} = \frac{1}{A} \int_{cavity} \frac{\|\nabla \theta\|^2}{(1 + \theta \Delta T / T_0)^2} dx dz \quad (6)$$

It was demonstrated that in steady-state the number of total irreversibility (conductive plus viscous) and the Nusselt number must always be equal. This identity cannot be obtained when the work of pressure forces is neglected in the model, see (Pons and Le Quéré, 2005a, 2005b). The second thermodynamic quantity considered herein is the number of viscous irreversibility, N_{Iv} .

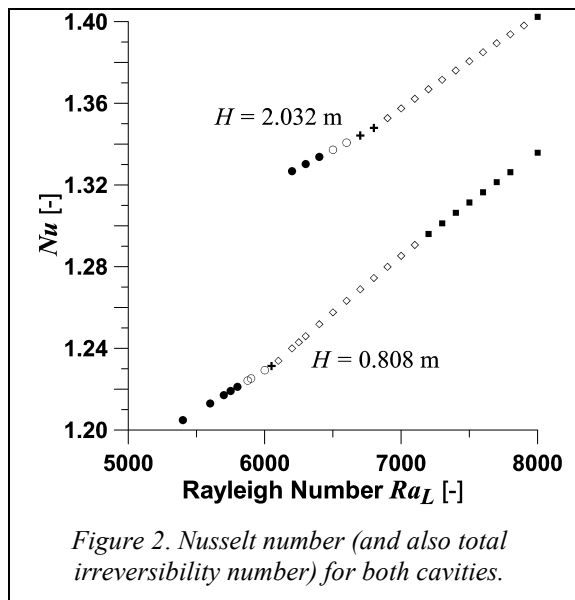


Figure 2. Nusselt number (and also total irreversibility number) for both cavities.

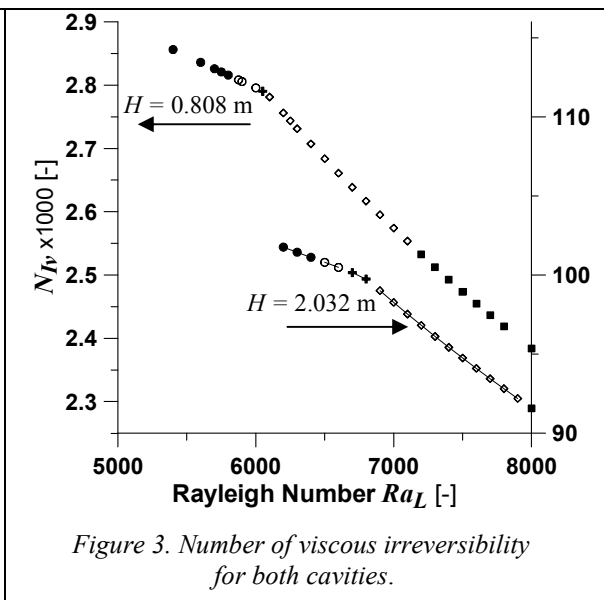


Figure 3. Number of viscous irreversibility for both cavities.

The symbols display the number of secondary cells : ● : no secondary cell, ○ : 2 secondary cells, + : 4, ◇ : 6 and ■ : 7 secondary cells.

Those three features are due to the work of pressure forces (Pons and Le Quéré, 2007). Indeed this work acts as a heat sink in the rising boundary layer (the hot one) and a heat source in the other one, see the term $-\phi w$ in Equation (3). These heat sink and heat source have two effects. First, they induce a direct heat transfer from the vicinity of the hot wall to that of the cold wall; this is how heat transfer is increased. Second, they reduce the average temperature difference between the two boundary layers. The latter effect reduces the buoyancy forces, which results in a less intense convection at given Rayleigh number; this is why viscous friction is reduced. Moreover this less intense convection makes the flow more stable,

Figure 2 presents the Nusselt number and Figure 3 the number of viscous irreversibilities N_{Iv} in the investigated Rayleigh-range. As shown in Equation (5), N_{Iv} is scaled by the parameter ϕ . This parameter differs by a factor of 40 between the two cavities. For sake of comparison, Figure 3 is presented with two ordinate axes, one for each cavity, their respective scales being in that ratio of 40.

1.1. Comparison between the two cavities

Comparing the *large* cavity to the *small* one, three main features can be observed in Figures 2 and 3. Heat transfer is non-negligibly increased (approx. +6%); viscous irreversibility is reduced, significantly before transition, non-negligibly after; and transition occurs at significantly higher values of Ra_L (approx. +12%).

shifting the transition to multi-cellular flow toward higher values of the Rayleigh number.

These simple observations show that the work of pressure forces, always neglected in *usual* Boussinesq calculations, can play a quantitative role (increased heat transfer) and also a qualitative one (increased stability) in configurations that belong to daily life (two-meter high a cavity).

1.2. Description of the transition

Two secondary cells appear at the center of the *small* (resp. *large*) cavity at $Ra_L=5875$ (resp. 6500), in agreement with the linear stability analyses. However, the thermodynamic analysis leads to a different threshold. Each curve Nu and

N_{IV} vs. Ra_L , Figures 2 and 3, displays only **one** knee, located at $Ra_L=6100$ (resp. 6800), *i.e.* when the flow skips from four to six secondary cells. None of the other topology changes, *e.g.* from one to two cells, or from six to seven cells, produces discontinuity on those curves. Is just the presence of secondary cells, regardless of their size, the relevant signature of transition? Why is the change from four to six cells more important than the other changes?

At transition, the Nusselt number presents a *relative* increase (*i.e.* the slope after transition is larger than before), a well known feature (Lee and Korpela, 1983; ElSherbiny et al., 1983; Lartigue et al., 2000; Wright et al., 2006). Because of this *relative* increase in heat transfer, it is sometimes argued that transition occurs because the system would, by principle, tend to maximize heat transfer. Then why do not the secondary cells appear at lower Rayleigh numbers, when they would also increase heat transfer?

As can be seen in Figure 3, transition also corresponds to a *relative* decrease of viscous irreversibility (*i.e.* the slope after transition is less than before), a feature that was never commented before and makes a deeper thermodynamic analysis necessary.

Thermodynamic analysis

The stability analyses mentioned in introduction have shown that the perturbation (the “cats eyes”) is driven by the base flow via the Reynolds stresses (Bergholz, 1978). However, the base flow in the cavity is not one-dimensional like in those stability analyses, but two-dimensional due to confinement by the horizontal walls, see Figure 1. Thus all the secondary cells are not identical, their width decreases when going from the center to the ends, see the rightmost frame in Figure 1. In addition, all the secondary cells are encompassed into one streamline that separates the mono-cellular flow outside and the multi-cellular flow inside.

Let us first study the reduction of viscous friction induced by the multi-cellular flow. It is rather obvious that rolls, even co-rotating, offer less resistance than shear along a line. The Kelvin-Helmholtz instability also involves this resistance lowering. However, the topology generated by the unequal cells increases this effect.

Figure 4 presents the flow topology in the *small* cavity with $Ra_L=6500$ (the figure is very similar for the *large* cavity). There are six secondary cells. Attention is now focused on the streamline separating the mono-cellular and multi-cellular flows. It appears that this streamline

($\psi=-2.052 \times 10^{-3}$ bold black line) actually forms two large sub-cells containing all the secondary cells and with only one node where velocity vanishes and shear is maximal (at the center of the cavity), while at the other end of those sub-cells ($z \approx 0.2$ and 0.8) there is no discontinuity and the internal multi-cellular flow is directly driven by the external mono-cellular flow. The same pattern is repeated at the next level: each of those two sub-cells is again sub-divided in two sub-cells of second level ($\psi=-2.088 \times 10^{-3}$ bold dark red line); again there is only one node with zero velocity and maximal shear, and no discontinuity at the other end. A third level of sub-division exists (bold blue line $\psi=-2.154 \times 10^{-3}$), with same pattern.

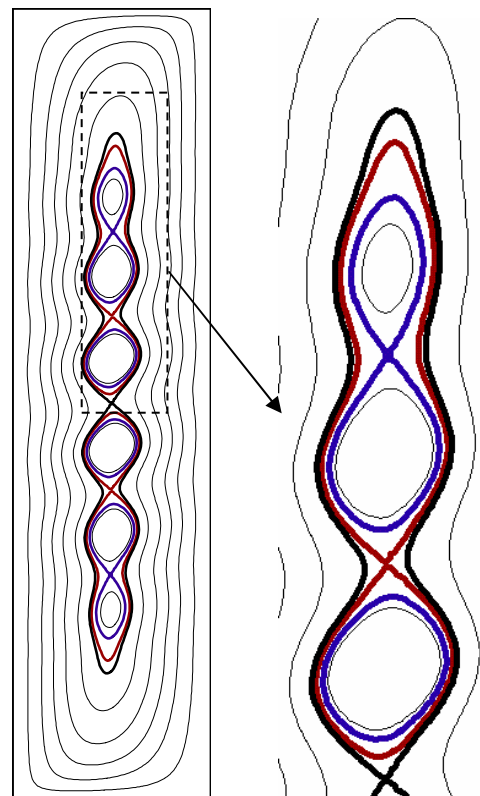


Figure 4. Streamlines in the small cavity at $Ra_L=6500$. Values of -1000ψ from 0.2 to 2.2 by steps of 0.4 for the thin lines, plus 2.0520, 2.088 and 2.154 for the bold lines. On the right: zoom on the upper half of the multi-cellular flow. The figures are expanded fivefold horizontally for clarity.

In such a topology, each sub-cell undergoes direct friction with only one of its neighbors, whatever its level. This topology also contributes to the *relative* decrease of viscous friction shown in Figure 3. As this overlapping arrangement was not found by stability analyses, it is very likely due

to the presence of the horizontal walls. Some previous numerical studies had already shown streamlines with such an arrangement (Roux et al., 1980; Lee and Korpela, 1983; Le Quéré, 1990), but none had commented on it.

Let us now study heat transfer. It is well known that the secondary cells increase heat transfer by producing an alternation of spots with high and low heat-fluxes along the vertical walls (Lartigue et al., 2000; Zhao et al., 1997).

Looking now at irreversibilities, *Figure 3* shows that transition makes viscous irreversibility decrease *relatively*, and (remembering that at steady-state $Nu = N_{Iv} + N_{Iq}$) total irreversibility increase *relatively*. It results from this relation and those changes that conductive irreversibility N_{Iq} *relatively* increases, and it increases more than total irreversibility -and Nusselt number- do. Transition thus clearly modifies how the two types of irreversibility distribute: it induces more conduction and less friction. *Figure 5* presents the field of local conductive irreversibility in the central part of the cavity (*i.e.* for $0.2 < z < 0.8$). The dashed line is the isovalue 1, *i.e.* the *locus* where local conductive irreversibility equals that in the purely conductive system (fluid at rest). In the darkest regions, conductive irreversibility lies between 1.25 and 1.75, in the clearest regions it is less than 0.75. It must be remembered that conductive irreversibility is highly

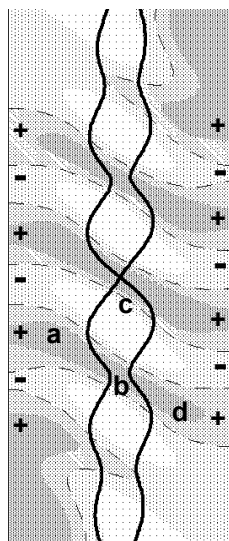


Figure 5. Local conductive irreversibility in the central portion of the cavity ($0.2 < z < 0.8$) with the bold streamline separating the mono- and multi-cellular flows. Same case as in Figure 4; figure also expanded fivefold horizontally.

non-uniform and reaches very high values (18 in the case shown in *Figure 5*.) in the bottom-left and top-right corners (not shown in *Figure 5*). We focus on the central part of the cavity, there where the secondary cells form. *Figure 5* shows how the uniform temperature gradient of the *conduction* regime is distorted by the secondary cells. The already-known alternation of regions with high and low heat-fluxes on the vertical walls clearly appears (positions '+' and '-') but this graph also shows that the secondary cells create shortcuts for conductive transfer from the hot to the cold wall. There are two main ideas for describing the new heat transfer configuration: each secondary cell produces a heat sink for the hot wall and a heat source for the cold wall, the secondary cells force the main flow to sway.

It first can be seen that the regions with high heat-fluxes ('+') are located almost at same height, slightly upwind, as the cell centers: indeed constriction of the main flow mechanically enhances horizontal temperature gradients. Heat flux is practically horizontal from the wall to the middle of boundary layer (position 'a' in *Figure 5*). Beyond the boundary layer, conductive heat-flux veers upwind of the flow toward a node of secondary cells (position 'b' in *Figure 5*). There, the heat flux separates in two parts: one part is advected by the flow inside the secondary cell from the bottom of the secondary cell ('b') to its top ('c') where it is released by conduction to the sinking main flow; the other part just diffuses by conduction toward the cold boundary layer through the node of the secondary cells ('b'), where the fluid velocity is very low. This conductive input into the sinking boundary layer locally increases temperature, so that the next constriction of main flow induces a region of high conductive heat transfer through the boundary layer and toward the cold wall (position 'd'). The final path is again horizontal.

This description leads to several comments. First comment: the swaying character of the main flow is as important as recirculation inside the secondary cells for the new heat transfer and flow configuration. Second and trivial comment: the flow topology affects the temperature field and the mechanisms of heat transfer. The third comment returns to thermodynamics: a change in the temperature field affects in return production of mechanical energy by the buoyancy forces. Indeed, the above-described heat-sinks and -sources created by the secondary cells globally decrease (resp. increase) the average temperature of the rising hot (resp. sinking cold) boundary layer. These temperature changes obviously *relatively*

increase the Nusselt number, but also they have another consequence: the buoyancy forces are reduced, and so is the mechanical work they produce. This work, which is the very source of fluid motion in the cavity, is the integral of the product of the buoyancy force $\beta g \rho_0 (T - T_0)$ by the vertical component of velocity V_z . Introducing the non-dimensional variables, the local rate of buoyancy work produced per unit volume is $\frac{k \beta g \Delta T}{c_p L} \sqrt{ARa_L} w \theta$. Integration over the 2-D cavity yields the total buoyancy work:

$$W_b = \frac{k \Delta T A H \beta g}{c_p} \sqrt{ARa_L} \int_0^1 \int_0^{1/A} w \theta dx dz \quad (7)$$

For the sake of consistency with the definition of the Nusselt number, the buoyancy work is non-dimensionalized with respect to the heat flux in the purely conductive system $Ak\Delta T$, yielding the corresponding number:

$$N_{Wb} = \sqrt{ARa_L} \frac{\beta g H}{c_p} \int_0^1 \int_0^{1/A} w \theta dx dz \quad (8)$$

where one can recognize the product $\frac{\beta g H}{c_p} w \theta$

which is the very last term of Equation (3). When the specific effects of the Rayleigh number via $\sqrt{ARa_L}$ and of the cavity size via $\frac{\beta g H}{c_p}$ are

eliminated, then the *small* and *large* cavities can be compared on a common basis. We therefore consider the quantity $\overline{N}_{Wb} = \int_0^1 \int_0^{1/A} w \theta dx dz$.

Figure 6 presents the changes of \overline{N}_{Wb} with the Rayleigh number for both cavities. It is remarkable how this graph unambiguously displays one transition, and only one. It can be interpreted as follows. It first must be remembered that, as the size of each cavity is fixed, the Rayleigh number is increased via the temperature difference imposed on the vertical walls. This temperature difference is the external constraint the flow is submitted to.

Before transition (mono-cellular flow), increasing the external constraint (ΔT and Ra) increases altogether the buoyancy forces, flow intensity, shear along the centerline of the cavity, mechanical work generated by the buoyancy forces and viscous friction. These two quantities grow more rapidly than $\sqrt{Ra_L}$ (*i.e.* than the factor scaling the reference velocity, see Section 2). Figure 6 shows that this behavior is not affected at all by the onset of two and then four secondary cells.

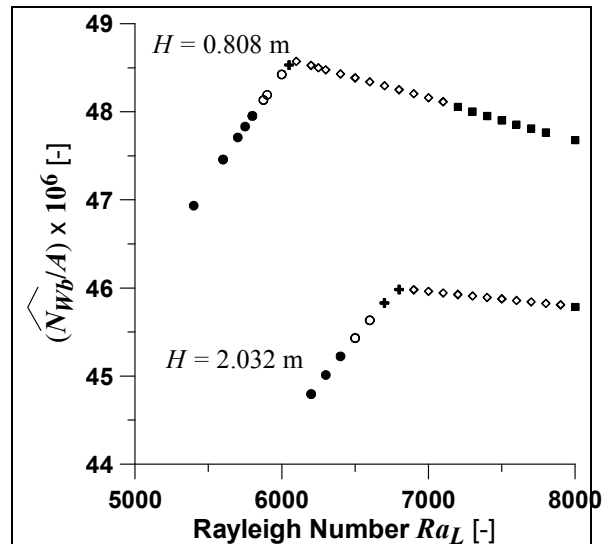


Figure 6. Non-dimensional buoyancy work for both cavities. Same symbols as in Figures 2 and 3.

Transition occurs very sharply and between four and six secondary cells. This transition does not change much the intensity of the external mono-cellular flow (*cf.* Figure 1: the streamlines in the cavity ends are hardly changed by transition) but makes secondary rolls replace shear flow along the center line AND the boundary layers sway.

After transition, an increase in Rayleigh intensifies circulation more in the secondary cells than in the main flow, and in parallel strengthens deformation of the external main flow. The negative slopes observed after transition in Figure 6 mean that both viscous friction and work of buoyancy forces increase less than $\sqrt{Ra_L}$. On the one hand rolls offer less resistance than shear, and on the other hand swaying tends to reduce temperature difference between the boundary layers, *i.e.* buoyancy forces.

When the number of secondary cells jumps from six (even) to seven (odd), the slopes in Figure 6 are hardly modified.

One aspect of this behavior looks paradoxical: the secondary cells tend to weaken the intensity of convection, although this is the cause that makes them exist. However, thermodynamics describes transition differently. First, as only steady-states are involved in this transition, the basic thermodynamics rule is that work of buoyancy forces always exactly counterbalances viscous dissipation. Second, before transition, the larger the Rayleigh number, the more intense convection in the cavity, and the stronger shear along the center line. As rolls offer less resistance than shear along a line, the flow tends to generate rolls. However, rolls can exist

only when the external main flow is strong enough for sustaining them despite the swaying, just like in the Kelvin-Helmholtz problem. Once they exist, the rolls modify heat transfer through the boundary layers in such a way that the buoyancy work decreases in full accordance with the decrease in flow resistance (balance between buoyancy work and viscous friction). This is the reason why a threshold exists.

This analysis shows that the increase in global heat transfer is just a by-product and not the main cause of transition. Transition appears then, not as a process that would maximize heat transfer, but as a threshold between two different ways of exactly balancing buoyancy work (where couples thermal and convective phenomena) with viscous dissipation:

- before transition: buoyancy work of straight boundary layers *vs.* viscous dissipation of linear shear, both grow more rapidly than $\sqrt{Ra_L}$;
- after transition: buoyancy work of swaying boundary layers *vs.* viscous dissipation of rolls, both grow less rapidly than $\sqrt{Ra_L}$.

Coupling between the temperature- and velocity fields, *i.e.* non-linear phenomena, plays a major role in that threshold.

2. Conclusion

This work leads to a double conclusion. First, the work of pressure forces is not negligible in configurations that can easily be met in building engineering (2.5m high rooms) provided the temperature differences are small enough, for instance close to equilibrium. Those forces quantitatively increase heat transfer and reduce convection, so that transition is delayed. Such configurations are correctly simulated with the *thermodynamic* Boussinesq model only. Second, the transition between mono- and multi-cellular flows can be explained in details by thermodynamic analysis. Instead of maximization of heat transfer, transition appears as a threshold between two ways of balancing the work of buoyancy forces and viscous dissipation. The thermodynamic analysis also explains why the threshold exists.

Acknowledgement

The numerical calculations were done on the NEC-SX8 of CNRS-IDRIS, Orsay, France.

Nomenclature

A aspect ratio, $A=H/L$
 c_p specific heat at constant pressure [$J.kg^{-1}.K^{-1}$]

g gravity acceleration [$m.s^{-2}$]
 H cavity height [m]
 k fluid thermal conductivity [$W.m^{-1}.K^{-1}$]
 L cavity width [m]
 N_I number of irreversibility
 Nu Nusselt number
 P pressure [Pa]
 Pr fluid Prandtl number
 q_v heat generated by viscous friction [$W.m^{-3}$]
 Ra_L Rayleigh number based on the cavity width
 t time [s]
 T temperature [K]
 ΔT temperature difference $\Delta T=T_h-T_c$ [K]
 u non-dimensional horizontal velocity
 V_z vertical velocity [$m.s^{-1}$]
 w non-dimensional vertical velocity
 W mechanical work [W]
 x non-dimensional horizontal coordinate
 z non-dimensional vertical coordinate

Greek letters

α fluid thermal diffusivity [$m^2.s^{-1}$]
 β thermal expansion coefficient [K^{-1}]
 ϕ non-dimensional adiabatic temperature gradient
 Φ non-dimensional viscous heat rate
 ρ fluid density [$kg.m^{-3}$]
 θ non-dimensional temperature
 τ non-dimensional time
 ν fluid kinematic viscosity [$m^2.s^{-1}$]
 ψ non-dimensional stream-function

Indexes

b buoyancy
 c cold wall
 h hot wall
 q conduction
 v viscous
 0 reference

References

- Batchelor, G. K., 1954, "Heat Transfer by Free Convection across a Closed Cavity Between Vertical Boundaries at Different Temperatures", *Quarterly of Applied Mathematics*, Vol. 12, No. 3, pp. 209-233.
- Bergholz, R. F., 1978, "Instability of Steady Natural Convection in a Vertical Fluid Layer", *J. Fluid Mech.*, Vol. 84, No. 4, pp. 743-768.
- Betts, P. L. and Bokhari, I. H., 2000, "Experiments on Turbulent Natural Convection in an Enclosed Tall Cavity", *Int. J. Heat and Fluid Flow*, Vol. 21, No. 6, pp. 675-683.
- Birikh, R. V., 1966, "On Small Perturbations of a Plane Parallel Flow with Cubic Velocity Profile",

- Applied Mathematics and Mechanics*, Vol. 30, pp. 432-438.
- Birikh, R. V., Gershuni, G. Z., Zhukhovitskii, E. M., and Rudakov, R. N., 1968, "Hydrodynamic and Thermal Instability of a Steady Convective Flow", *Applied Mathematics and Mechanics*, Vol. 32, No 2, pp. 246-252.
- Birikh, R. V., Gershuni, G. Z., Zhukhovitskii, E. M., and Rudakov, R. N., 1969, "Stability of the Steady Convective Motion of a Fluid With a Longitudinal Temperature Gradient", *Applied Mathematics and Mechanics*, Vol. 33, pp. 937-947.
- Boussinesq, J., 1903, *Théorie Analytique de la Chaleur*, Gauthier-Villars, Paris.
- Chait, A. and Korpela, S. A., 1989, "The Secondary Flow and Its Stability for Natural Convection in a Tall Vertical Enclosure", *J. Fluid Mech.*, Vol. 200, pp. 189-216.
- Costa, V. A. F., 2005, "Thermodynamics of Natural Convection in Enclosures with Viscous Dissipation", *Int. J. Heat Mass Transfer*, Vol. 48, No 11, pp. 2333-2341.
- De Vahl Davis, G. and Mallinson, G. D., 1975, "A Note on Natural Convection in a Vertical Slot", *J. Fluid Mech.*, Vol. 72, No. 1, pp. 87-93.
- Desrayaud, G. and Lauriat, G., 1988, "Radiative Influence on the Stability of Fluids Enclosed in Vertical Cavities", *Int. J. Heat Mass Transfer*, Vol. 31, No. 5, pp. 1035-1048.
- Elder, J. W., 1965, "Laminar Free Convection in a Vertical Slot", *J. Fluid Mech.*, Vol. 23, No. 1, pp. 77-98.
- ElSherbiny, S. M., Raithby, G. D., and Hollands, K. G. T., 1982, "Heat Transfer by Natural Convection Across Vertical and Inclined Air Layers", *J. Heat Transfer*, Vol. 104, No. 1, pp. 96-102.
- Gray, D. D. and Giorgini, A., 1976, "The Validity of the Boussinesq Approximation for Liquids and Gases", *Int. J. Heat Mass Transfer*, Vol. 19, No. 5, pp. 545-551.
- Korpela, S. A., Gözüüm, D., and Baxi, C. B., 1973, "On the Stability of the Conduction Regime of Natural Convection in a Vertical Slot", *Int. J. Heat Mass Transfer*, Vol. 16, No. 9, pp. 1683-1690.
- Lartigue, B., Lorente, S., and Bourret, B., 2000, "Multicellular Natural Convection in a High Aspect Ratio Cavity: Experimental and Numerical Results", *Int. J. Heat Mass Transfer*, Vol. 43, No. 17, pp. 3157-3170.
- Leonard, B. P., and Drummond, J. E., 1995, "Why you should not use 'Hybrid', 'Power-Law' or Related Exponential Schemes for Convective Modelling - there are much better Alternatives", *Int. J. Numerical Methods in Fluids*, Vol. 20, No. 6, pp. 421-442.
- Le Quéré, P., 1990, "A Note on Multiple and Unsteady Solutions in Two-Dimensional Convection in a Tall Cavity", *J. Heat Transfer*, Vol. 112, No. 4, pp. 965-974.
- Lee, Y. and Korpela, S. A., 1983, "Multicellular Natural Convection in a Vertical Slot", *J. Fluid Mech.*, Vol. 126, pp. 91-121.
- Pons, M. and Le Quéré, P., 2005a, "An Example of Entropy Balance in Natural Convection, Part 1: the Usual Boussinesq Equations", *Comptes Rendus Mecanique*, Vol. 333, No. 2, pp. 127-132.
- Pons, M. and Le Quéré, P., 2005b, "An Example of Entropy Balance in Natural Convection, Part 2: the Thermodynamic Boussinesq Equations", *Comptes Rendus Mecanique*, Vol. 333, No. 2, pp. 133-138.
- Pons, M. and Le Quéré, P., 2007, "Modeling Natural Convection With the Work of Pressure-Forces: a Thermodynamic Necessity", *Int. J. Numerical Methods for Heat and Fluid Flow*, Vol. 17, No. 3, pp. 322-332.
- Roux, B., Grondin, J. C., Bontoux, P., and De Vahl Davis, G., 1980, "Reverse Transition From Multicellular to Monocellular Motion in Vertical Fluid Layer", *Europhysics Conf. Madrid March 30-April 2, 1980*, Thomas, G., European Physical Society, Geneva, Switzerland, Vol. 3F, pp. 292-297.
- Spiegel, E. A. and Veronis, G., 1960, "On the Boussinesq Approximation for a Compressible Fluid", *Astrophys. J.*, Vol. 131, pp. 442-447.
- Velarde, M. G. and Perez-Cordon, R., 1976, "On the (Non-linear) Foundations of Boussinesq Approximation Applicable to a Thin Layer of Fluid. II. Viscous Dissipation and Large Cell Gap Effects", *J. de Physique*, Vol. 37, No. 3, pp. 177-182.
- Vest, C. M. and Arpaci, V. S., 1969, "Stability of Natural Convection in a Vertical Slot", *J. Fluid Mech.*, Vol. 36, No 1, pp. 1-15.
- Wright, J. L., Jin, H., Hollands, K. G. T., and Naylor, D., 2006, "Flow Visualization of Natural Convection in a Tall, Air-Filled Vertical Cavity", *Int. J. Heat Mass Transfer*, Vol. 49, No. 5-6, pp. 889-904.
- Zhao, Y., Curcija, D., and Goss, W. P., 1997, "Prediction of the Multicellular Flow Regime of Natural Convection in Fenestration Glazing Cavities", *ASHRAE Transactions*, Vol. 103, No. 1, pp. 1-12.